Formation and statistical properties of rogue wave in dispersion-managed fiber lasers

Yueqing Du, Qun Gao, Chao Zeng, Dong Mao,* and Jianlin Zhao

Key Laboratory of Light Field Manipulation and Information Acquisition, Ministry of Industry and Information Technology, MOE Key Laboratory of Material Physics and Chemistry under Extraordinary Conditions, and Shaanxi Key Laboratory of Optical Information Technology, School of Physical Science and Technology, Northwestern Polytechnical University, Xi'an 710129, China

(Received 22 March 2021; revised 12 May 2021; accepted 18 May 2021; published 4 June 2021)

Rogue wave in ultrafast fiber lasers is a hot research topic of nonlinear optics, which is generally monitored at the fixed cavity positions, despite its dramatic intra-cavity evolution. The shot-to-shot statistical properties change significantly if the chaotic pulse experiences strong changes along the cavity, which is rarely considered in the past. Here, we simulate the dynamic evolution of the rogue wave in the dispersion-managed fiber laser. Attributing to the temporal structure change induced by the dispersion, the rogue wave within the noise-like pulse appears in a limited cavity region while disappears in the rest parts. It is also demonstrated that the dispersion is capable of manipulating rogue waves in the pulse trains outside the cavity. Our results offer insightful views on the properties of chaotic waves in ultrafast lasers.

DOI: 10.1103/PhysRevA.103.063504

I. INTRODUCTION

Ultrafast fiber laser can emit dissipative-soliton (DS) through mode locking, which is widely used in industry and science [1]. The DS in the ultrafast laser may lose its coherence when suffering strong nonlinearity and instability such as the noiselike pulse (NLP) [2,3]. The NLP is a temporal wave packet containing many internal fine structures, which can be incoherent or partially coherent depending on the laser settings [4–8]. The formation mechanism of the NLP is attributed to the peak-clamp effect or the soliton collapse [5,6]. Although some general properties of the NLP have been revealed, it is still a mysterious object because we can't "see" the internal structures due to the limited resolution of the measurement; especially, extreme events such as optical rogue waves (RWs) are found to be linked with the chaotic properties of the NLP [9–11].

Originally, the RW is used to describe the extreme wave in the turbulent ocean [12] that is harmful to human sailings. In nonlinear optical systems, the RW refers to the rare event accompanied by extreme intensity or energy enhancement during the light wave evolution. The probability density function (PDF) of the light waves has a long tail at the side of high amplitude if RWs emerge [13]. Soli *et al.* found the RW generation at the long wavelength during the supercontinuum generation ascribed to the ejection of rogue solitons. Usually, the RW in the supercontinuum arises from the Raman soliton collision under delicate conditions [14,15]. The noise-seeded modulation instability (MI) in optical fibers, where the wave propagation can be described by the nonlinear Schrodinger equation (NLSE), can trigger the collisions between Akhmediev breathers, resulting in extreme intensity enhancement [16–19]. In addition to the breather collisions, soliton collisions are capable of generating the RW during the MI evolution if the initial condition is properly set [20]. Overall, collisions between multiple wave components can trigger the RW generation in the conservative and quasiconservative optical systems.

The dissipative systems with gain and dissipative terms to exchange energy with environments, such as fiber lasers, are also capable of generating the RWs. Pulses in mode-locked lasers will degenerate into a chaotic wave-packet containing internal fine structures and subpulses, such as the chaotic pulse bunch, multiple solitons, and NLPs with different time scales. Experiments and simulations demonstrate that collisions between pulses inside the complex wave packet can induce the RW [11,21–23]. Some nontrivial mechanisms of the RWs in addition to the collision have also been proposed. Slow dynamics of the saturable absorber (SA) of the laser can induce the ultrafast RWs [24]. Dispersive waves can evolve into RWs after being strongly amplified [25]. In the buildup of mode locking, the RW arises from the transient amplification of the DS [26]. In the unstable mode-locked fiber laser, the nonlinear focusing process of a pulse can enhance its peak power, resulting in the RW [27,28]. These results demonstrate that pulse collisions, wave amplification, and temporal focusing are three common pathways to enhance the light wave. In addition to the temporal RW, several spectral RWs have been observed experimentally while their underlying mechanisms remain to be fully explored [29,30]. The discovery, exploration, and progress of RWs in optical systems are clearly summarized in the reviews [31].

The pulse experiences strong breathing along the cavity of dispersion-managed (DM) fiber laser, manifesting as the position-related properties [13,32–34]. The ultrafast laser resembles a black box that can only be measured through the shot-to-shot wave evolution at discrete output ports, and the intracavity evolution is like a huge iceberg hidden under the water. If the NLP brings RWs in the DM laser, a

*Corresponding author: maodong@nwpu.edu.cn

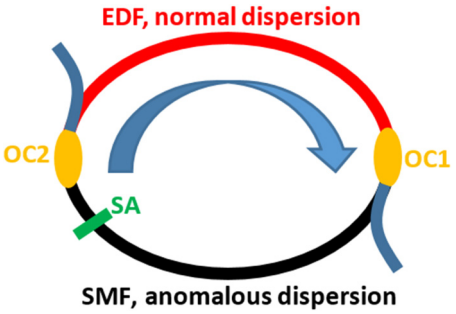

FIG. 1. Schematic configuration of the ultrafast DM fiber laser in the simulation. EDF: Er-doped fiber; OC: output coupler; SMF: single-mode fiber; SA: saturable absorber.

natural question is whether the shot-to-shot evolution of the NLP has distinct statistical properties along the cavity. This is rarely addressed in the literature, especially important for the optical systems with discrete components, which is the main content of this paper. The DM technique is widely used in optical communication links, fiber amplifiers, and lasers, and thus studying the RW is helpful for improving the quality and stability of these optical systems.

In this paper, we reveal the RW dynamics about NLP in the DM ultrafast fiber laser based on the lumped model with discrete components. For the NLP propagation in the anomalous-dispersion fiber, the evolution is turbulent and a rogue pulse will appear randomly due to temporal focusing. Interestingly, the RW disappears in the normal-dispersion fiber due to the coherence recovery. The dramatic evolution of the NLP in the cavity results in distinct temporal structures at different output ports. It demonstrates that the dispersion of fiber is the key factor to control the temporal structures of the NLP and RW. Our work paves the way for understanding and controlling extreme events in ultrafast fiber lasers.

II. MODEL FOR SIMULATIONS

The schematic configuration of the fiber laser is shown in Fig. 1, which comprises 2.5-m Er-doped fiber (EDF) and 6.81-m single-mode fiber (SMF) to ensure the zero net dispersion of the cavity. The EDF and SMF have group velocity dispersion of 60 and $-22\,\mathrm{ps}^2/\mathrm{km}$, respectively. The Kerr nonlinear parameters of the EDF and SMF are 8.67 and $1.3\,\mathrm{W}^{-1}\,\mathrm{km}^{-1}$, respectively. The setting for the parameters of the SMF and EDF are based on SMF-28 and the RightWave EDF80 (OFS) in reality, demonstrating the available experimental implementation of our proposed numerical model. Two output couplers (OCs) are placed at the end of the EDF and SMF, where shot-to-shot statistical properties of the wave are recorded. The SA is placed 0.2 m in front of OC2. In reality, the linear loss of the cavity can be induced by two OCs, splicing between fibers, and the intrinsic loss of the fiber. However, as a proof of concept, to simplify the model and highlight the scope of this work, we concentrate all linear losses at OC1 (10% output coupling). Despite that the results are obtained with the initial condition of a weak pulse, we have checked the case with the white noise as the initial condition, whose final results have no intrinsic difference

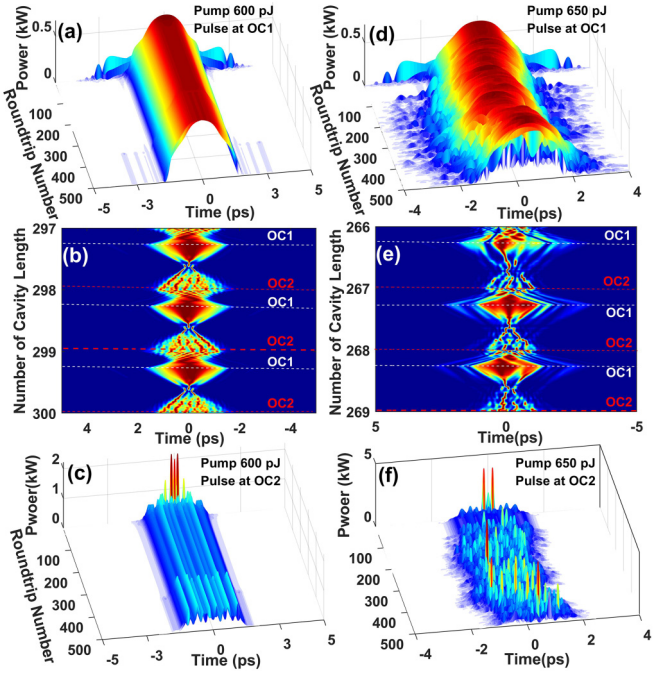

FIG. 2. Shot-to-shot evolutions of the pulses at two OCs under different pump energies. Pump energy of 600 pJ: (a) Shot-to-shot evolution at OC1. (b) Intracavity evolution from the 298th to 300th RT. (c) Shot-to-shot evolution at OC2. Pump energy of 650 pJ: (d) Shot-to-shot evolution at OC1. (e) Intracavity evolution from the 267th to 269th RT. (f) Shot-to-shot evolution at OC2.

with the results in this paper. The pulse propagation in the laser is described by the generalized NLSE and solved by the symmetric split-step Fourier method,

$$\frac{\partial u}{\partial z} = -i\frac{\beta_2}{2}\frac{\partial^2 u}{\partial t^2} + \frac{g-l}{2}u + i\gamma|u|^2 u + \frac{g}{2\Omega_g{}^2}\frac{\partial^2 u}{\partial t^2}, \quad (1)$$

$$g = g_0 \exp\left(-\int_0^{T_r} |u|^2 dt/E_s\right), \quad (2)$$

$$T = 1 - \alpha/(1+P/P_s), \quad (3)$$

where u is the amplitude of the pulse, g is the gain of the EDF, E_s is a phenomenological parameter to represent the pump energy of the EDF, T_r is the width of the time window, t is the amplitude transmission function of SA, P is the instantaneous power of the optical pulse, α and P_s are the modulation depth and saturable power of the SA, which are set as 0.7 and 100 W, respectively. In the SMF, g is set to be zero in Eq. (1).

III. SIMULATION RESULTS

A. Shot-to-shot evolution of the NLP

In Figs. 2(a)–2(c), at the pump strength of 600 pJ, the pulse holds a coherent shot-to-shot evolution at two OCs. In a previous work [35], the high-order soliton evolution is found to be a stable state in the DM fiber laser at high pump energy, which is obvious in the intracavity evolution [Fig. 2(b)]. After the quasistationary evolution from the 1st to 357th roundtrip (RT), the pulse bifurcates into a period-2 evolution after the

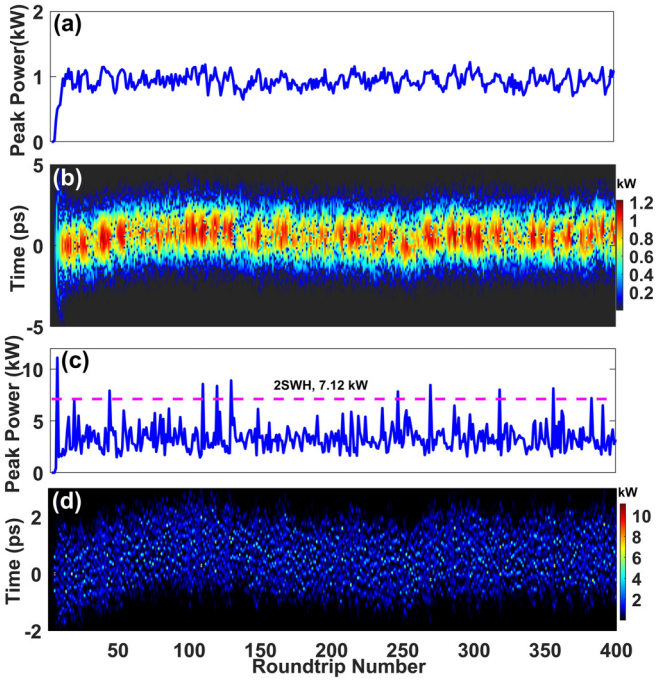

FIG. 3. Shot-to-shot evolutions of the pulse at two OCs at the pump energy of 1470 pJ. (a) Peak power evolution at OC1. (b) Shot-to-shot evolution at OC1. (c) Peak power evolution at OC2. (d) Shot-to-shot evolution at OC2.

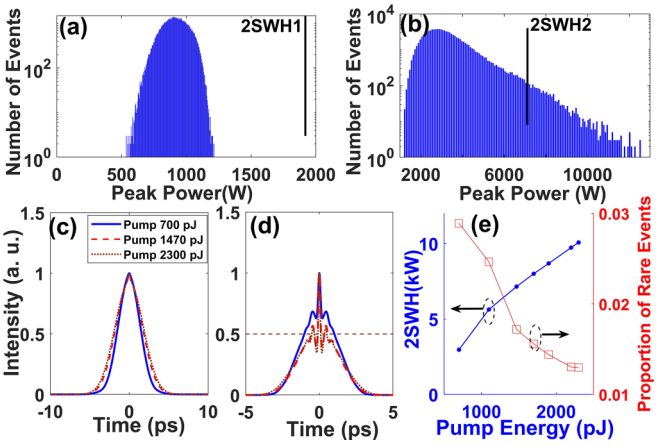

FIG. 4. Statistical properties of the pulse trains at two OCs with net-zero dispersion. (a) PDF at OC1 with 1470-pJ pump energy. (b) PDF at OC2 with 1470-pJ pump energy. (c) Average ACTs at OC1 with three different pump energies. (d) Average ACTs at OC2 with three different pump energies. (e) Dynamics of threshold and proportion of RWs at different pump energies.

357th RT. At OC2, the pulse has multiple peaks [Fig. 2(c)]. The distinct features of the pulse at two OCs can be understood through the intracavity evolution in Fig. 2(b). In each circulation of the intracavity evolution, the pulse at the end of the EDF has a soliton order higher than 3, experiencing the nonlinear compression and subsequent pulse breaking in the SMF. After the broken pulse re-enters EDF at the next RT, it is recovered to a coherent pulse benefitting from the normal-dispersion EDF. Thereby, the pulse at the end of EDF (OC1) is smooth while it is structured at the end of the SMF due to the high-order soliton effect. In Figs. 2(d)–2(f), by increasing the pump strength to 650 pJ, the pulse at OC2 is a typical NLP consisting of many fine structures. Some extreme peaks emerge during the pulse evolution at OC2, which can be regarded as the RW. The distinct shot-to-shot evolutions of two OCs can be understood through the dramatic intracavity evolution as shown in Fig. 2(e).

To force the NLP evolution to be more stochastic, the pump energy is increased to 1470 pJ and the NLP evolutions at two OCs are shown in Fig. 3. The peak power of the NLP at OC1 fluctuates chaotically within a small range in Fig. 3. The NLP at OC1 in Fig. 3(b) manifests as a bright pulse embedded with temporal dips. We have checked that the dark structures have typical properties of dark solitons, similar to those emerging during the soliton explosion [34]. RW is absent in the shot-to-shot evolution at OC1 in consecutive 200 000 RTs. Different from the case at OC1, RWs emerge at OC2, as shown in Fig. 3(c). We count the peak power of the wave packet for each RT, then the significant wave height (SWH) is defined as the average value of the highest third of the shot-to-shot evolution over 200 000 RTs, and the pulse with the peak power that overcomes two times the SWH is defined as an RW. Such definition and calculation of the RW have been implemented experimentally in lasers [21,29]. There is a different statistical approach in [22] that counts all the local maximum peaks within a chosen time box of the chaotic wave packet. The trivial difference between the definitions doesn't affect the main features of RW, i.e., rarity and extreme. The RW thresholds for the pulses at OC1 and OC2 in Fig. 3 are 1.9 and 7.12 kW, respectively. Several RWs emerge during the first 400 RTs at OC2, as shown in Fig. 3(c), wherein the peak power evolution is more stochastic than that in Fig. 3(a). The chaotic pulse at OC2 in Fig. 3(d) is a wave packet with many bright structures, which differs from the smooth pulse embedded with dark solitons at OC1 [Fig. 3(b)].

The PDFs of the shot-to-shot evolution for the peak power at two OCs are shown in Fig. 4. In Fig. 4(a), the maximum of the counted peak power at OC1 is far from its threshold of RW. At OC2, the PDF has a long tail that overcomes the threshold of RW. This is an interesting phenomenon, i.e., the RW emerges at OC1 while it disappears at OC2 in the ultrafast fiber laser with DM. The average autocorrelation traces (ACTs) of the pulse intensity at OC1 for three different pump energies are shown in Fig. 4(c). The central peak of ACT is almost invisible in Fig. 4(c), which is distinct from the tradition NLP with a narrow peak on its ACT [2], indicating the internal correlation of the pulse at OC1. This is reasonable because the NLP at OC1 is a smooth pulse instead of the stochastic wave packet. The ACTs at OC2 have a strong peak located on the wide pedestal, which is the typical characteristic of the NLP. At the pump energy of 700 pJ, the height ratio of the central peak is smaller than 0.5, which demonstrates the partially internal correlation between the subpulses in the NLP.

For the larger pump energy, the height ratio of the central peak reaches 0.5, indicating the irrelevance of fine structures inside the NLP. At OC2, the threshold of the RW increases with the enhancement of the pump energy. Oppositely, the proportion of the rare events decreases with the increase of the

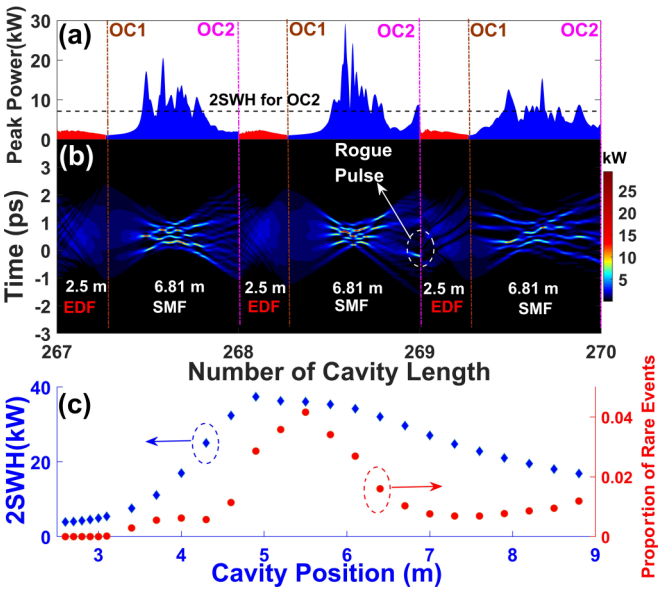

FIG. 5. Intracavity dynamics at the pump energy of 1470 pJ and zero net dispersion. (a) Peak power of the wave packet at each cavity position from the 268th to 270th RT. (b) Intracavity evolution of the temporal intensity profile of the wave packet from the 268th to 270th RT. (c) Statistical properties of the wave packet for different cavity positions. Diamonds: thresholds of RW at the corresponding cavity position. Dots: proportion of RWs over 200 000 RTs at the corresponding cavity position.

pump energy, as shown in Fig. 4(e). This is because the higher the threshold of the RW, the more difficult for the pulse to be increased to an RW. Before the NLP splits into multiple NLPs at the pump energy of 2400 pJ, the RW always exists at OC2 while it vanishes at OC1.

B. Intracavity wave evolution

To better understand the shot-to-shot evolution in Figs. 2–4, we shed light on the intracavity dynamics from the 268th to 270th RT (Fig. 5), where the RW for OC2 emerges within the 269th RT as marked in Fig. 5(b). The NLP in the cavity breathes twice over one RT due to the DM effect, which is similar to that of the stretch pulse [33–35]. From Fig. 5(a), one can find that the peak power of the pulse in the EDF at different RTs has a small fluctuation while it evolves dramatically in the SMF. In each RT, the peak power of the pulse exceeds that of the threshold of RW for OC2 at some positions of SMF, which implies that the shot-to-shot statistical property of the pulse is position dependent. We can see from Fig. 5(b) that the NLP experiences the pulse-breaking-recovery inside the EDF [35], which recovers the smooth profile at OC1. The smooth pulse narrows in the SMF and splits into a wave packet consisting of many subpulses. After the wave packet reaches the minimum width, it broadens and splits into clustered subpulses. The cascading splitting is similar to the behavior of high-order-soliton in Fig. 2(b). When the pulse arrives at the OC2, it manifests as an NLP with subpulses. The pulse at OC2 reaches the threshold of RW in the 269th RT as marked in Figs. 5(a) and 5(b).

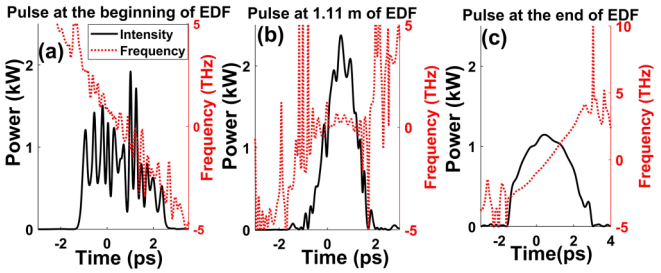

FIG. 6. Pulse states three cavity positions in the EDF in the 269th RT: (a) Pulse state at the beginning of the EDF. (b) Pulse state at 1.11 m of the EDF. (c) Pulse state at the end of EDF.

In Fig. 5(b), the pulse evolves stochastically in the middle part of the SMF. Intuitively, the shot-to-shot evolution of the pulse is more turbulent if the OC locates in this region of cavity positions. We calculate the shot-to-shot statistical properties (over 200 000 RTs) at different positions along the cavity [Fig. 5(c)]. No RW emerges in the forepart of the cavity (3 m), wherein the pulse keeps a smooth profile without strong subpulses. After the smooth pulse is distorted into many subpulses [Fig. 5(b)] in the SMF, with the narrowing of the wave packet, the subpulses have more chance to be enhanced to an RW, thus the proportion of the RW increases with the cavity position from 3 to 5.5 m [Fig. 5(c)]. The largest probability of the RW is 4.16% at the cavity position of 5.5 m. After the narrowest state of the NLP, the wave packet begins to stretch, reducing the intensity of the subpulses as well as their chances to develop into an RW. Thereby, the probability of the RW decreases to 0.69% at the position of 7.3 m. Although the wave packet broadens in the SMF, for one of the subpulses inside the NLP, it might accumulate an up-chirp of frequency due to the self-phase modulation (SPM) and cross phase modulation (XPM) among adjacent subpulses, which induce the nonlinear temporal focusing so that the subpulse is enhanced to an RW. In this way, the probability of the RW turns to increase after the position of 7.3 m and reaches 1.72% at the end of the SMF. The threshold for the RW increases to 37.43 kW at the cavity position of 4.9 m and then decreases to 7.15 kW at the end of the SMF, which agrees with the breathing behavior of the pulse in the SMF [Fig. 5(b)]. The results in Fig. 5(c) indicate that the shot-to-shot statistical properties of the NLP depend on the intracavity evolution.

C. Mechanism of RW and pulse shaping

We take the NLP evolution in the EDF within the 269th RT as an example to analyze why the pulse at OC1 is smooth. The NLP in Fig. 6(a) at the beginning of the EDF is a wave packet consisting of many subpulses, accompanied with a nonlinear down-chirp. After a propagating distance of 1.11 m, the NLP is narrowed while its internal subpulses are suppressed as shown in Fig. 6(b). The chirp across the NLP is still nonlinear but near zero in the center of the NLP. Then, the pulse becomes smooth with a linear up-chirp at the end of the EDF. The transition of the frequency chirp from the nonlinear to the quasilinear state facilitates the pulse-breaking-recovery evolution. The linear chirp makes the pulse smooth while the nonlinear chirp distorted the pulse as a

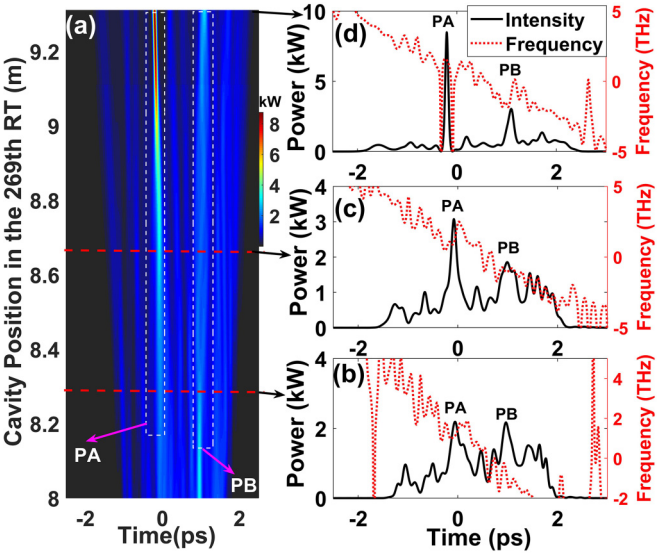

FIG. 7. Pulse states three cavity positions in the EDF in the 269th RT: (a) Pulse state at the beginning of the EDF. (b) Pulse state at 1.11 m of the EDF. (c) Pulse state at the end of EDF.

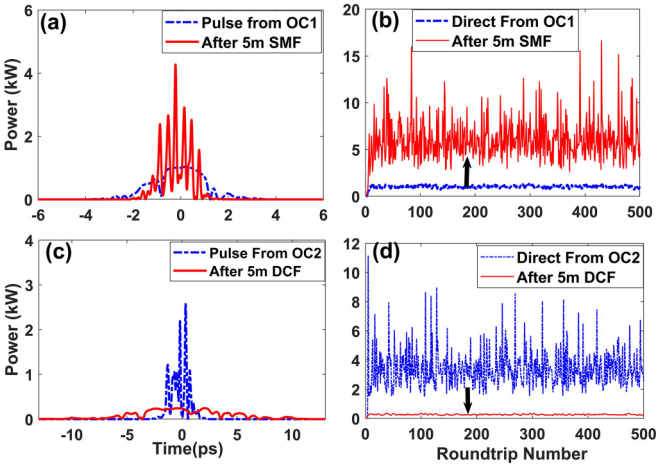

FIG. 8. (a) Single-shot pulse at the 500th RT from OC1 and its profile at propagation in 5-m SMF. (b) Shot-to-shot evolutions of the peak power direct from OC1 and after propagation in 5-m SMF. (c) Single-shot pulse at the 500th RT from OC2 and its profile at propagation in 5-m DCF. (d) Shot-to-shot evolutions of the peak power direct from OC2 and after propagation in 5-m DCF.

structured NLP. With the nonlinear chirp, one frequency component is distributed in the temporal domain with different temporal locations as well as different phases, whose internal interference produces complex patterns in the temporal domain. It can also be understood through the wave-breaking theory: when the pulse has a nonlinear chirp, the temporal lagging long-wavelength component will pass through the temporal leading short-wavelength component in the normal-dispersion regime, resulting in the local oscillating temporal structures. The normal dispersion of the EDF compensates the nonlinear down-chirp induced by the Kerr nonlinearity of SMF, recovering the chirp of the pulse to be a quasilinear up-chirp as shown in Fig. 6(c). The chirp at the edges of the pulse is nonlinear in Fig. 6(c), which results in the distorted patterns. Due to the overall smoothing state at the end of EDF, it is impossible to generate an extreme peak at OC1, indicating the disappearance of RW at OC1.

Another important issue is how the RW emerges at OC2. When the NLP propagates in the SMF, one can see two strong subpulses marked by PA and PB in Fig. 7(a). At 8.31 m, PA and PB have the up- and down-chirps in their central parts [Fig. 7(b)], respectively. The anomalous dispersion narrows PA while it broadens PB in conjunction with their chirps. The evolution of PA and PB is dominated by the dispersion rather than the nonlinearity because the dispersion lengths are much shorter than the nonlinear lengths. PA is increased in power and narrowed in width while PB is weakened and broadened at 8.65 m [Fig. 7(c)]. When PA and PB reach the OC2 in Fig. 7(d), PA evolves into a strong pulse, which is an RW in the pulse train outputted from OC2. Thus, the rogue pulse is caused by the temporal focusing effect.

Different from the *up-chirp* of the subpulse that evolves into an RW in the anomalous-dispersion SMF, the wave packet after its narrowest state continues to spread in the temporal domain, indicating the overall *down-chirp* across the NLP. In this case, its internal subpulses such as PA or PB tend to have the down-chirp. However, the PA owns the up-chirp, which can only be induced by the SPM and the XPM by its adjacent subpulses. The XPM from the adjacent pulse is chaotic considering the dramatic evolution of the total wave packet, which makes the up-chirp for one subpulse (such as PA) a rare event.

D. Manipulation of RWs

The intracavity evolutions of the NLP reveals that the shot-to-shot evolution of the wave is more stochastic after passing through the SMF while the case is opposite after the EDF with normal dispersion, which inspires us to control the RW in the pulse train outside the laser cavity through the fiber or medium with dispersion. As a proof of concept, we inject the smooth pulse from OC1 (pump energy of 1470 pJ) into a segment of SMF, transforming the smooth pulse into the NLP with several strong subpulses, which is shown in Fig. 8(a). In addition, as shown in Fig. 8(b), the shot-to-shot evolution transforms into a turbulent state with extreme peaks after passing through the SMF. On the contrary, the profile of the NLP from OC2 becomes smooth after propagating in the DCF with a normal dispersion of 190 ps^2/km, accompanied by the transformation from the turbulent evolution into the moderate state, which is shown in Figs. 8(c) and 8(d). One can obtain from Fig. 8 that, despite the stochasticity of the wave patterns emitted from the cavity, their internal structures can be controlled outside the cavity through dispersion, demonstrating a flexible method of generating or erasing the RWs in the pulse trains.

IV. DISCUSSION

In conservative systems such as the noise-seeded MI in SMF, the dynamics of the RW can be effectively controlled by the initial conditions [13–20]. In our dissipative system, the small noise will be absorbed by the SA during the buildup process of ultrafast pulse, so the statistical RW is insensitive

to the initial and external noise. The pulse inside the fiber laser experiences several balances to ensure the quasi-self-consistent state, such as the gain and loss, spectral broadening and narrowing, and temporal stretching and compressing. In reality, we can only measure the shot-to-shot wave dynamics at discrete positions of the laser cavity despite the dramatic intracavity evolution. If one investigates the dissipative RW based on ultrafast lasers that should be described by the lumped model, the measuring position should be taken into account, otherwise one may miss the RW if it exists.

The pulse presented in this work maintains the "incoherent" state that refers to the chaotic evolution and clear collapse of the pulse structure, which is different from the instability in [36–38]. The pulse continuously switches between the NLP and "coherent soliton" in a chaotic manner, which is named "intermittence" and "breathing soliton explosion" in [36–38], respectively. We speculate that some rare events with extreme energy or intensity can emerge during the switching process of intermittence.

It has been experimentally revealed in both quasicontinuous-wave and mode-locked fiber lasers that the RWs have polarization-dependent features [24,39]. The nonlinearity-induced polarization coupling (both coherent and incoherent) will change the intensity and phase of the pulse or wave packet that circulates in the laser cavity. In addition, interactions between polarized components in the active fiber (such as the polarization burn hole) can affect the gain dynamics for pulses. With the increase of the degree of freedom for the incoherent pulse containing RWs, the vector properties of the RWs deserve to be further explored.

V. CONCLUSION

In this paper, we have simulated the shot-to-shot evolutions and statistical properties of the dissipative RWs in DM ultrafast fiber lasers. In the normal-dispersion part, the chaotic wave packet recovers its coherence accompanying with the disappearing of RW. It is shown that in the anomalous-dispersion part, some subpulses inside the NLP can be enhanced to an RW with extreme peak power in some RTs. The intracavity evolution of the wave has an important influence on the shot-to-shot statistics of the chaotic wave in the dissipative system, which is different from that in the conservative system. Our results provide a distinctive perspective for the understanding the dissipative RWs in ultrafast fiber lasers, which is helpful for manipulating the formation of extreme events in optical systems.

ACKNOWLEDGMENTS

This work was supported by the National Key R&D Program of China (Grant No. 2017YFA0303800), the National Natural Science Foundation of China (Grants No. 11634010 and No. 11874300), and the Fundamental Research Funds for the Central Universities (Grants No. 3102019JC008 and No. 3102019PY002).

[1] P. Grelu and N. Akhmediev, Nat. Photonics **6**, 84 (2012).
[2] M. Horowitz, Y. Barad, and Y. Silberberg, Opt. Lett. **22**, 799 (1997).
[3] A. F. J. Runge, C. Aguergaray, N. G. R. Broderick, and M. Erkintalo, Opt. Lett. **38**, 4327 (2013).
[4] Y. Kwon, L. A. Vazquez-Zuniga, S. Lee, H. Kim, and Y. Jeong, Opt. Express **25**, 4456 (2017).
[5] Z. Cheng, H. Li, and P. Wang, Opt. Express **23**, 5972 (2015).
[6] D. Y. Tang, L. M. Zhao, and B. Zhao, Opt. Express **13**, 2289 (2005).
[7] O. Pottiez, Y. E. Bracamontes-Rodriguez, H. E. Ibarra-Villalon, J. C. Hernandez-Garcia, M. Bello-Jimenez, J. P. Lauterio-Cruz, E. Garcia-Sanchez, and E. A. Kuzin, Laser Phys. **28**, 085108 (2018).
[8] S. Smirnov, S. Kobtsev, S. Kukarin, and A. Ivanenko, Opt. Express **20**, 27447 (2012).
[9] Z. Liu, S. Zhang, and F. W. Wise, Opt. Lett. **40**, 1366 (2015).
[10] S. V. Smirnov, S. Sugavanam, O. A. Gorbunov, and D. V. Churkin, Opt. Express **25**, 23122 (2017).
[11] P. Wang, D. Hu, K. Zhao, L. Jiao, X. Xiao, and C. Yang, IEEE J. Sel. Top. Quantum Electron. **24**, 1800207 (2018).
[12] A. L. Islas and C. M. Schober, Phys. Fluid **17**, 031701 (2005).
[13] D. R. Solli, C. Ropers, P. Koonath, and B. Jalali, Nature (London) **450**, 1054 (2007).
[14] J. M. Dudley, F. Dias, M. Erkintalo, and G. Genty, Nat. Photonics **8**, 755 (2014).
[15] A. Antikainen, M. Erkintalo, J. M. Dudley, and G. Genty, Nonlinearity **25**, R73 (2012).
[16] N. Akhmediev, A. Ankiewicz, and J. M. Soto-Crespo, Phys. Rev. E **80**, 026601 (2009).
[17] N. Akhmediev, J. M. Soto-Crespo, and A. Ankiewicz, Phys. Lett. A **373**, 2137 (2009).
[18] N. Akhmediev, J. M. Soto-Crespo, and A. Ankiewicz, Phys. Rev. A **80**, 043818 (2009).
[19] B. Frisquet, B. Kibler, and G. Millot, Phys. Rev. X **3**, 041032 (2013).
[20] J. M. Soto-Crespo, N. Devine, and N. Akhmediev, Phys. Rev. Lett. **116**, 103901 (2016).
[21] C. Lecaplain, Ph. Grelu, J. M. Soto-Crespo, and N. Akhmediev, Phys. Rev. Lett. **108**, 233901 (2012).
[22] J. M. Soto-Crespo, Ph. Grelu, and N. Akhmediev, Phys. Rev. E **84**, 016604 (2011).
[23] J. Peng, N. Tarasov, S. Sugavanam, and D. Churkin, Opt. Express **24**, 21256 (2016).
[24] A. Klein, G. Masri, H. Duadi, K. Sulimany, O. Lib, H. Steinberg, S. A. Kolpakov, and M. Fridman, Optica **5**, 774 (2018).
[25] S. Lee, K. Park, H. Kim, L. A. Vazquez-Zuniga, J. Kim, and Y. Jeong, Opt. Express **26**, 11447 (2018).
[26] Z.-C. Luo, J.-Q. Kang, M. Liu, C. Li, C.-H. Kong, Y. Yu, and K. K. Y. Wong, IEEE Photon. Tech. Lett. **30**, 1803 (2018).
[27] A. Zaviyalov, O. Egorov, R. Iliew, and F. Lederer, Phys. Rev. A **85**, 013828 (2012).

[28] W. Chang, J. M. Soto-Crespo, P. Vouzas, and N. Akhmdiev, Opt. Lett. **40**, 2949 (2015).
[29] M. Liu, A.-P. Luo, W.-C. Xu, and Z.-C. Luo, Opt. Lett. **41**, 3912 (2016).
[30] S. Chowdhury, B. Gupta, S. Chatterjee, R. Sen, and M. Pal, Opt. Lett. **44**, 2161 (2019)
[31] J. M. Dudley, G. Genty, A. Mussot, A. Chabchoub, and F. Dias, Nat. Phys. Rev. **1**, 675 (2019); Y. Song, Z. Wang, C. Wang, K. Panajotov, and H. Zhang, Adv. Photonics **2**, 024001 (2020).
[32] K. Tamura, E. P. Ippen, H. A. Haus, and L. E. Nelson, Opt. Lett. **18**, 1080 (1993).
[33] H. A. Haus, K. Tamura, L. E. Nelson, and E. P. Ippen, IEEE J. Quantum Electron. **31**, 591 (1995).
[34] Y. Du, X. Shu, H. Zhang, and P. Cheng, Opt. Express **26**, 11685 (2018).
[35] Y. Du, M. Han, and X. Shu, Opt. Lett. **45**, 666 (2020).
[36] C. Lapre, C. Billet, F. Meng, P. Ryckzowski, T. Sylvestyre, C. Finot, G. Genty, and J. M. Dudley, Sci. Rep. **9**, 13950 (2019).
[37] F. Meng, C. Lapre, C. Billet, G. Genty, and J. M. Dudley, Opt. Lett. **45**, 1232 (2020).
[38] J. Peng and H. Zeng, Phys. Rev. Appl. **12**, 034052 (2019).
[39] S. A. Kolpakov, H. Kbashi, and S. V. Sergeyev, Optica **3**, 870 (2016).